Summary

Three Anderson-Evans type polyoxomolybdate hybrid solids $[\{H\textit{pz}\}_2\{H_7CrMo_6O_{24}\}]\cdot 6H_2O$ (**1**), $[\{Cr_3(O)(CH_3COO)_6(H_2O)_3\}_2\{H_7CrMo_6O_{24}\}]\cdot 24H_2O$ (**2**) and $[Na\{Na(H_2O)_3\}_2\{H_6CrMo_6O_{24}\}]\cdot 2H_2O$ **(3)** have been crystallized via solvent evaporation technique in the presence of pyrazole (*pz*) as organic ligand. The solids were characterized using single crystal X-ray diffraction, fourier transform infrared spectroscopy and thermal analysis. While, solid **1** is an example of organically templated Anderson-Evans cluster based hybrid solid (Type I); in both **2** and **3** Anderson cluster is stabilized due to inorganic cationic moieties. Crystal structure analysis of **1**-**3** suggested that supramolecular interactions facilitate the crystal packing in synthesized solids. The role of synthetic parameters in dictating the nature of self-assembly of solids in aqueous medium was analyzed and the potential of solids **1**-**3** for the synthesis of Polypyrrole or Polypyrrole composite using chemical oxidative polymerization of pyrrole was examined.

II.1 Introduction

Self-assembly of hybrid solids involves a spontaneous aggregation of molecular precursors usually driven by metal-ligand coordination and supramolecular interactions such as hydrogen bonding, π···π and C-H···π interactions [1, 2]. However, synthetic parameters such as temperature, pH, metal ions, nature of organic ligand and solvent can alter the nature of the reacting molecular precursors. Therefore, subtle changes in reaction parameters can affect the aggregation of molecular precursors in the reaction medium, which in turn, affects the crystallization of hybrid solids [3-6]. Polyoxometalates, particularly Anderson–Evans cluster based solids provide an excellent opportunity to explore these issues as they can form a large variety of hybrid solids ranging from organically templated cluster based solids to coordination polymer incorporated cluster anions forming extended 3-D architectures [7, 8].

Anderson-Evans cluster has the general formula $[H_x(XO_6)M_6O_{18}]^{(9-x)-}$, where x = 6-7, M = addenda atoms (Mo^{VI}) and X = a central heteroatom [9]. Since, it can incorporate various heteroatoms, inorganic and organic cations and molecules exhibiting various coordination modes, it serves as an attractive building block for the crystallization of hybrid solids having rich topology, intriguing physico-chemical properties and diverse applications [10-13]. In addition, Anderson-Evans cluster specifically exhibits a relatively high tendency to undergo protonation and incorporate a large number of lattice water molecules during crystallization [14-16]. However, there are only limited examples of organically templated Anderson-Evans cluster based solids reported in literature (refer Table II.1).Therefore, in the present work an attempt has been made to synthesize Anderson-Evans cluster based solids using organic ligands and understand the role of synthetic parameters in dictating the nature of self-assembly in aqueous medium. The results are significant as such analysis provides clues for engineering new solids with

desired structure and dimensionality. In addition, the use of Anderson solids, for the synthesis of Polypyrrole (Ppy) or Polypyrrole composite via oxidative polymerization has also been investigated.

Table II.1 Organically templated Anderson-Evans cluster based solids reported in literature.

S. No.	Solid	Cell parameters	Synthetic technique	Structural description	Ref.
1	$\{H\textit{pym}\}_2[\{H_7CrMo_6O_{24}\}]\cdot 2H_2O$ *pym*= pyrimidine	Triclinic *P*-1 *a* = 6.830(1) Å *b* = 10.159(1)Å *c* = 10.644(2) Å *α* = 76.922(3)° *β* = 74.540(3)° *γ* = 87.543(4)° Z = 1	Solvent evaporation method	Anderson-Evans cluster anions linked to a pair of protonated pyrimidine moieties through C-H⋯O forming a zig–zag 1-D chains.	16
2	$\{(H\textit{temed})_3\}[\{H_6CrMo_6O_{24}\}_2]\cdot 16H_2O$ *temed*= tetramethylethylenediamine	Monoclinic $P2_1/c$ *a* = 13.592(3) Å *b* = 21.475(5) Å *c* = 14.286(3) Å *α*= 90° *β* = 114.538(4)° *γ*=90° Z = 2	Solvent evaporation method	Organic amine links Anderson-Evans cluster into 1-D chains through N-H⋯O interactions.	16
3	$(BEDT\text{-}TTF)_4[Cr(OH)_6Mo_6O_{18}]\cdot 2H_2O$ BEDT-TTF= bis(ethylenedithio) tetrathiafulvalene]	Triclinic *P*-1 *a* = 5.9545(2) Å *b* = 16.3767(6) Å *c* = 21.8643(6) Å *α*= 110.829(2)° *β* = 91.262(2)° *γ* = 98.129(1)° Z = 1	Electrochemical synthesis	The cluster and the organic moieties are arranged alternatively leading to 1-D chains through H-bonding interactions.	17
4	$\{(N_2H_5CO)[(CH_3)_3N(CH_2)_2OH]_2\}[H_6CrMo_6O_{24}]\cdot 4H_2O$	Monoclinic $C2/c$ *a* = 13.707(3) Å *b* = 22.113(4) Å	Solvent evaporation method at	Anderson anion cluster is linked to a pair of choline molecules and one	18

		c =13.194(3) Å *α*=90° *β*= 109.73(3)° *γ*= 90° Z = 4	room temperature	protonated urea molecule leading to 3-D assembly via $N_{(urea)}$-H···O interactions.	
5	(4-H*ampy*)$_2$[H_3O]($H_7CrMo_6O_{24}$)·$2H_2O$ *ampy* = aminopyridine	Triclinic *P*-1 (no. 2) *a* = 7.951(5) Å *b* = 10.036(5) Å *c* = 10.345(5) Å *α*= 88.976(5)° *β*= 78.016(5)° *γ*= 86.207(5)° Z = 1	Hydrothermal synthesis	Protonated 4-aminopyridine moieties and H_3O^+ cations link Anderson polyoxoanions through N-H···O interactions forming a layered structure.	19
6	(H_3O)[(3-a*mpy*)$_2$($H_6CrMo_6O_{24}$)]·$3H_2O$	Triclinic *P*-1 *a* = 7.848(8) Å *b* = 10.180(10) Å *c* = 10.410(10)Å *α* = 88.031(3)° *β* = 78.308(2)° *γ* = 88.842(3)° Z = 1	Hydrothermal synthesis	Protonated 3-aminopyridines link the Anderson cluster anion through strong N-H···O interactions.	20
7	($C_4H_{10}NO$)$_3$[$H_6CrMo_6O_{24}$]·$4H_2O$	Triclinic *P*-1 *a* = 7.947 (4) Å *b* = 9.965 (5) Å *c* = 13.740 (7) Å *α* = 110.392 (1)° *β* = 102.921 (1)° *γ* = 90.635 (1)° Z = 1	Refluxed and cooled to room temperature, followed by solvent evaporation.	The cluster anion, organic cations and water molecules are linked by N-H···O and O-H···O interactions.	21
8	(H*bipy*)$_2$[$Cr(OH)_6Mo_6O_{18}$H](*bipy*) *bipy* = bipyridine	Triclinic *P*-1 *a* = 8.540 (5) Å *b*= 10.593 (5)Å *c*= 11.864 (5)Å *α* =74.901 (5)° *β* =85.216 (5)° *γ* = 88.651 (5)° Z= 1	Hydrothermal synthesis	$[Cr(OH)_6Mo_6O_{18}]^{3-}$ anion and three *bipy* molecules, two of which are protonated are linked via H-bonding interactions leading to supramolecular assembly.	22

II.2 Experimental

II.2.1 Synthesis

All reagents were of reagent grade and were used as received from commercial sources without further purification in the present thesis. The solids were synthesized using solvent evaporation technique, similar to that reported in literature [23]. Scheme II.1 summarizes the synthetic methodology employed in this study to prepare Anderson cluster based hybrid solids. Initially, two different aqueous solutions were prepared for the synthesis of **1**. Solution A was prepared by adding $Na_2MoO_4 \cdot 2H_2O$ (2.35 mmol, Merck, 99%) to a solution of $CrCl_3 \cdot 6H_2O$ (1.57 mmol, Merck, 99%) in 15 mL of water and 5 mL of glacial acetic acid. Solution B was prepared by adding pyrazole (2.52 mmol, Merck, 99%) to a solution of $CoCl_2 \cdot 6H_2O$ (1.68 mmol, Merck, 99%) in 10 mL of water and 10 mL of methanol. Subsequently, Solution **B** was added to Solution **A** and acidified using dilute HCl. The resultant green colored solution of pH ~ 2 was left for crystallization at room temperature. After 4 weeks, purple needle like crystals of **1** were obtained, filtered, washed with acetone and air dried. Yield: 72% (based on Mo).

When Solution **A** was left undisturbed at room temperature, dark green block like crystals of **2** were obtained after 3 weeks in about 54% yield (based on Mo). The crystals of **2** were washed with acetone, filtered and air dried. The filtrate upon evaporation at room temperature resulted in pink block like crystals of **3** after 2 weeks in about 32% yield (based on Mo). Using 2-aminopyrazine (2-*ampz*) instead of pyrazole resulted in crystallization of solid $[Co(2\text{-}H\textit{ampz})_2Cl_4]$, **4**, which is discussed in detail in Chapter III.

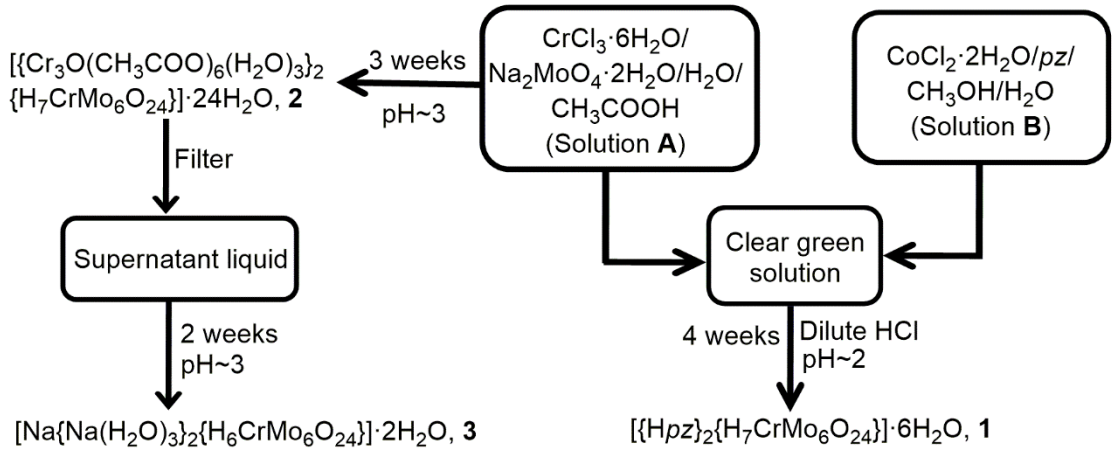

Scheme II.1 Scheme showing the synthetic pathway for the crystallization of solids **1-3**.

II.2.2 Synthesis of Polypyrrole using Anderson-Evans hybrid solids

To a stirring solution of 10 mL of $[\{Cr_3(O)(CH_3COO)_6(H_2O)_3\}_2\{H_7CrMo_6O_{24}\}].24H_2O$, **2** (0.03M), 0.5 mL pyrrole dissolved in 20mL of distilled water was added, followed by 0.02g of ammonium persulphate (APS). The contents were stirred for about 15 minutes and the resultant black powder was washed with distilled water, filtered and dried in oven at 50°C. The same procedure was repeated with solid **3**. Polypyrrole was also synthesized using only APS with the same concentration of pyrrole and APS as stated above.

II.2.3 Characterization

II.2.3.1 X-ray crystallographic studies

X-ray diffraction studies of crystal mounted on a capillary were carried out on a BRUKER AXS SMART-APEX diffractometer with a CCD area detector (MoKα = 0.71073Å, monochromator: graphite) [24]. Frames were collected at T = 298K (for **1**) and 293K (for **2** and **3**) by ω, ϕ and 2θ-rotation at 10s per frame with SAINT [25]. The measured intensities were reduced to F^2 and corrected for absorption with SADABS [25]. Structure solution, refinement, and data output were carried out with the SHELXTL

program [26]. Non-hydrogen atoms were refined anisotropically. C-H and N-H hydrogen atoms were placed in geometrically calculated positions by using a riding model. Images were created with the DIAMOND program [27]. Hydrogen bonding interactions in the crystal lattice were calculated with SHELXTL and DIAMOND [26, 27]. Crystal and refinement data have been summarized in Table II.2.

II.2.3.2 Powder X-ray diffraction

Powder X-ray diffraction **(**PXRD) data was collected on a Malvern Panalytical Aeris diffractometer using Ni-filtered CuKα radiation. Data were collected with a step size of 0.02° and count time of 2s per step over the range $5° < 2\theta < 60°$.

II.2.3.3 Fourier Transform Infrared Spectroscopy

Fourier transform infrared (FTIR) spectra were recorded using Shimadzu FTIR spectrophotometer (model: IR Affinity-1S) equipped with Attenuated total reflection (ATR) in the range 400-4000 cm^{-1}.

II.2.3.4 Thermogravimetric Analysis

Thermogravimetric analysis (TGA) was done on Perkin-Elmer TGA7 from room temperature to 900^{o}C at a heating rate of 10^{o}C/min. in nitrogen atmosphere to determine water and organic content as well as overall thermal stability of the products.

Table II.2 Crystal data and structure refinement parameters for **1-3**.

	1	**2**	**3**
Chemical formula	$C_6H_{22}CrMo_6N_4O_{30}$	$C_{24}H_{36}Cr_7Mo_6O_{80}$	$CrMo_6Na_3O_{32}$
Molecular weight	1257.91	2544.17	1208.61
Temperature (K)	298(2)	293(2)	293(2)
Crystal system	orthorhombic	Triclinic	Triclinic
Space Group	*Pbca*	*P*-1	*P*-1
a (Å)	23.1796(8)	10.1347(14)	6.4631(16)
b (Å)	11.1281(4)	14.688(2)	10.904(3)
c (Å)	25.1499(9)	15.442(2)	10.929(3)
α (°)	90.00	108.076(2)	109.100(4)
β (°)	90.00	93.539(2)	106.790(4)
γ (°)	90.00	92.825(2)	95.509(4)
Volume ($Å^3$)	6487.3(4)	2175.4(5)	681.1(3)
Z	8	1	1
ρcalc ($g \cdot cm^{-3}$)	2.576	1.942	2.700
μ (mm^{-1})	2.678	1.791	2.727
F (000)	4816	1240.0	1274
Crystal size (mm)	0.47 x 0.31 x 0.26	0.35 x 0.29 x 0.25	0.37 x 0.27 x0.22
Radiation	Mo *K*α	Mo *K*α	Mo *K*α
2Θ range for data collection (°)	4.12 to 56.280	2 to 60	2.08 to 50
Index ranges	$-28 \le h \le 30$, $-14 \le k \le 13$, $-33 \le l \le 29$	$-12 \le h \le 12$, $-17 \le k \le 17$, $-18 \le l \le 18$	$0 \le h \le 13$, $-12 \le k \le 13$, $-16 \le l \le 17$
Reflections collected	38438	20309	7773
Independent reflections	7911	7660	3380
Data/restraints/parameters	7911/0/442	7660/0/535	5549/0/433
Goodness-of-fit on F^2	1.061	1.051	1.125
$R[F^2 > 2\sigma(F^2)]$, $wR(F^2)$	0.0338, 0.0841	0.0313, 0.0954	0.0344, 0.0776

II.3 Results and Discussion

II.3.1 Crystal Structure of 1-3

II.3.1.1 Crystal Structure of 1

The asymmetric unit of **1** consists of one Anderson-Evans cluster anion, two protonated pyrazole moieties (designated as {N1N2} and {N3N4} hence forth) and six lattice water molecules. The crystal structure analysis of **1** revealed that Anderson-Evans cluster anion was identical to those reported in literature (Table II.1). The Anderson cluster anion *viz.* $[H_7CrMo_6O_{24}]$ was a B-type Anderson structure consisting of six $[MoO_6]$ octahedra arranged in a hexagonal manner around the central $[Cr(OH)_6]$ octahedron (FigureII.1). Each $[MoO_6]$ octahedra exhibited three kinds of Mo-O distances in **1**(Table II.3). These included molybdenum-terminal oxygen, Mo-Ot bonds (1.695(2)-1.709(2) Å) and two types of molybdenum bridging oxygen bonds namely Mo-Ob and Mo-Oc. While, Ob adopted a μ_2-bridging mode linking two adjacent molybdenum centers (1.892(2)-2.037(2) Å), Oc adopted μ_3-bridging mode linking two molybdenum centers and the central chromium atom (2.268(2)-2.314(2) Å). The bond-valence sum calculations [28] suggested that Cr was in +3 oxidation state, all Mo atoms were in the +6 oxidation state and seven oxygen atoms in **1** were protonated. Lattice water molecules namely O1S, O2S, O5S and O6S formed strong hydrogen bonds (Table II.4) with the cluster ions to form zig-zag 1-D chains propagating along *b* axis (FigureII.2). One of the pyrazole moieties *viz.* {N1N2} was linked to cluster anions via O1S through N-H···O interactions. O2S connected the 1-D chains via H-bonding interactions to form a sheet along *ab*-plane (FigureII.3). The sheets were further connected via lattice water molecules (O3S and O4S) and {N3N4} moiety to form 3-D supramolecular structure as shown in Figure II.4.

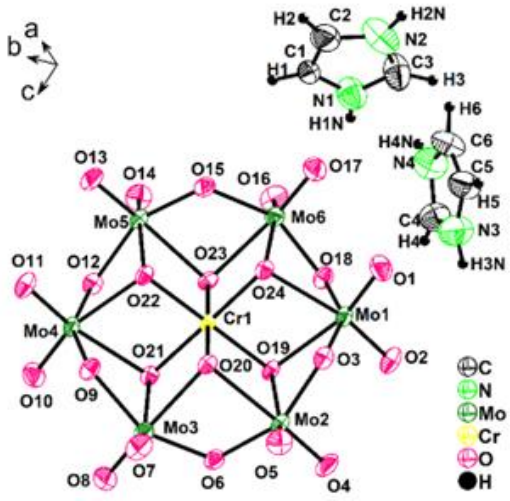

Figure II.1 ORTEP diagram of **1.** Non hydrogen atoms are shown as 50% ellipsoids and hydrogen atoms as arbitrary spheres. Lattice water molecules have been omitted for clarity.

Table II.3 Mo-O distances in **1**.

Category	Mo···O	Bond Distance (Å)
Molybdenum-terminal oxygen (Mo-Ot)	Mo1···O1	1.697(2)
	Mo1···O2	1.706(2)
	Mo2···O7	1.691(2)
	Mo2···O8	1.690(2)
	Mo3···O11	1.702(2)
	Mo3···O12	1.706(2)
	Mo4···O15	1.705(2)
	Mo4···O16	1.708(2)
	Mo5···O19	1.695(2)
	Mo5···O20	1.706(2)
	Mo6···O23	1.699(2)
	Mo6···O24	1.709(2)
Molybdenum-bridging oxygen (Mo-Ob)	Mo1···O6	1.946(2)
	Mo1···O3	1.936(2)
	Mo2···O6	1.905(2)
	Mo2···O9	2.037(2)
	Mo3···O9	2.028(2)
	Mo3···O13	1.899(2)
	Mo4···O13	1.986(2)
	Mo4···O17	1.892(2)
	Mo5···O17	1.961(2)
	Mo5···O22	1.915(2)
	Mo6···O22	1.932(2)
	Mo6···O3	1.946(2)

Molybdenum-internal oxygen (Mo-Oc)	Mo1···O4	2.280(2)
	Mo1···O5	2.303(2)
	Mo2···O5	2.299(2)
	Mo2···O10	2.273(2)
	Mo3···O10	2.272(2)
	Mo3···O14	2.268(2)
	Mo4···O14	2.274(2)
	Mo4···O18	2.287(2)
	Mo5···O18	2.299(2)
	Mo5···O21	2.314(2)
	Mo6···O21	2.300(2)
	Mo6···O4	2.279(2)

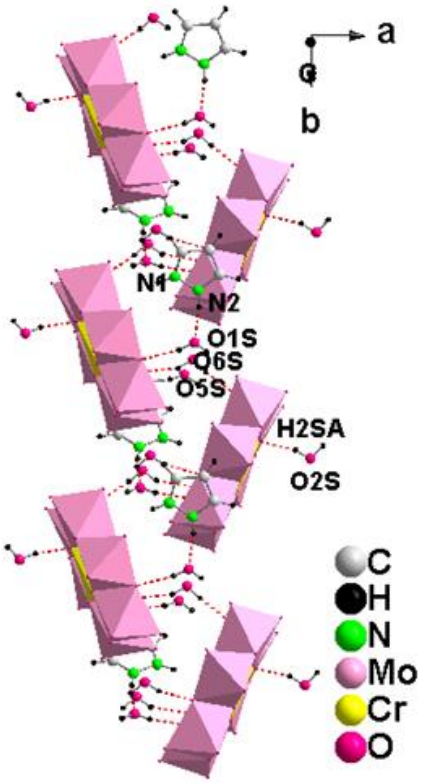

Figure II.2 1-D zig-zag chains in **1**. H-bonding interactions are shown in dashed red lines. Each cluster anion is linked to lattice water molecules O1S, O2S, O5S and O6S through H-bonding. Lattice water molecule, O1S is linked to {N1N2} moiety through N-H···O interaction.

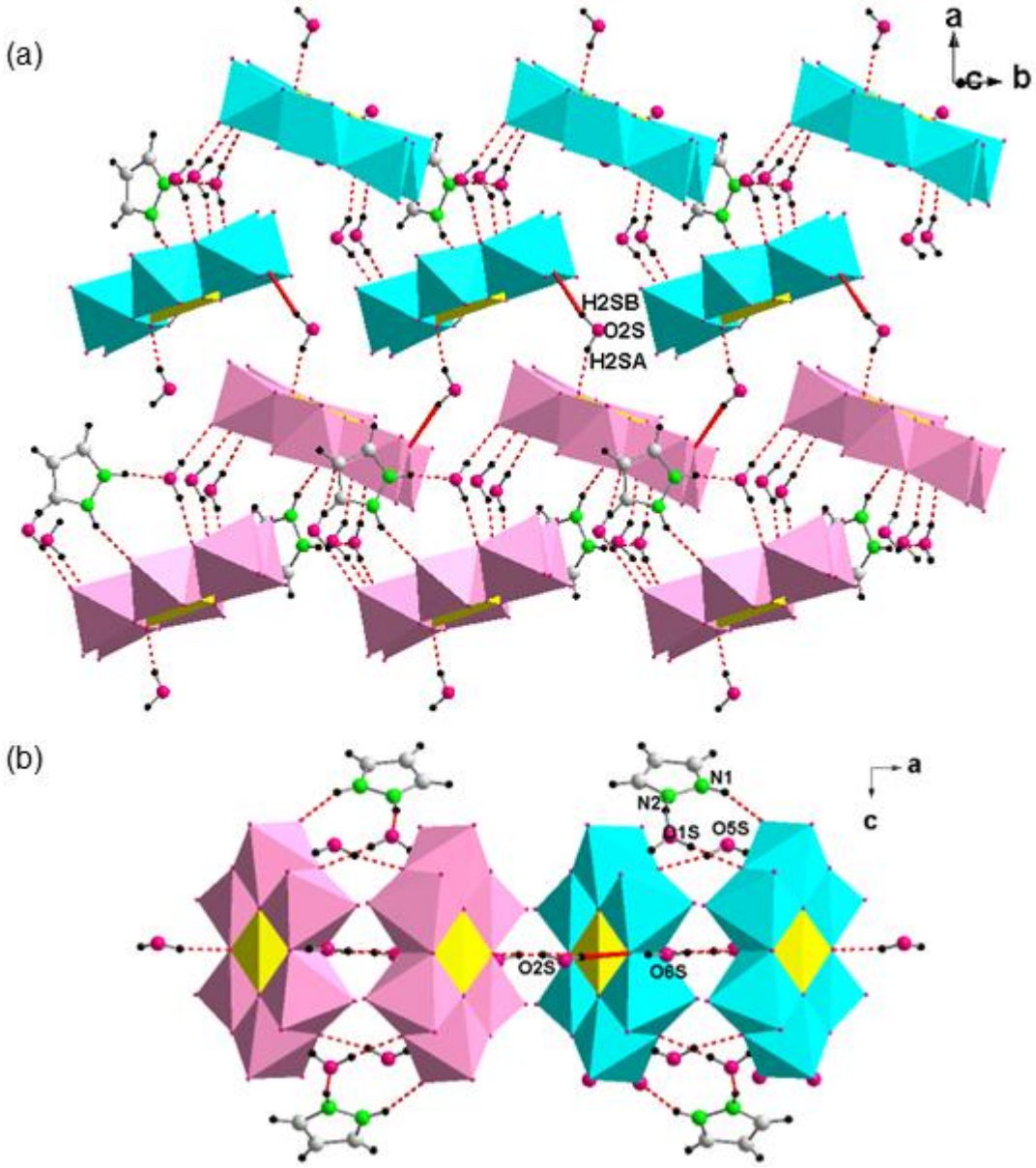

Figure II.3 (a) O2S connecting two neighboring 1-D zig-zag chains (depicted in cyan and pink polyhedral) to form 2-D sheet in **1**. Inter-chain H-bonding interactions are shown in solid red lines. (b) View along *b* axis showing two 1-D chains forming a sheet.

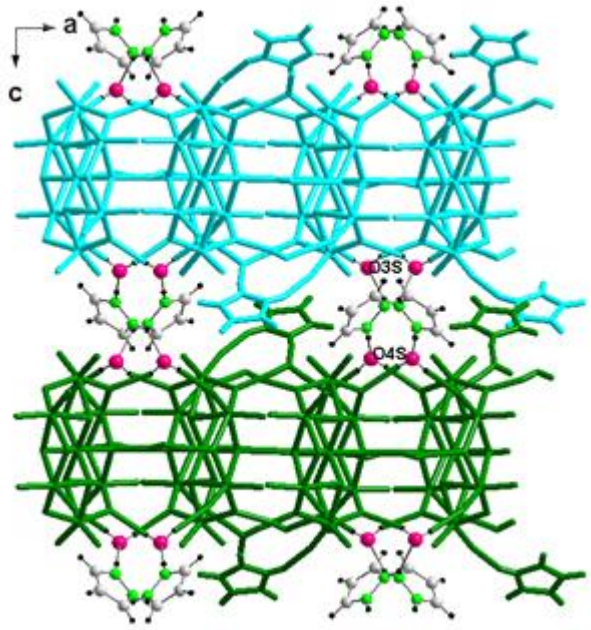

Figure II.4 View along *b* axis showing O3S and O4S connecting two neighboring sheets (depicted in cyan and green) via H-bonding interactions mediated by {N3N4} moiety in **1**.

Table II.4 H-bonding interactions in **1**.

D-H···A	**D-H (Å)**	**H···A (Å)**	**D···A (Å)**	**∠ D-H···A (°)**
O(1S)-H(1SA)···O15	0.8510(27)	1.9202(19)	2.7628(32)	170.3(1)
O(1S)-H(1SB)···O5	0.8500(27)	2.0211(23)	2.8657(36)	172.3(1)
O(2S)-H(2SA)···O19	0.8489(28)	1.7511(19)	2.5699(32)	161.4(1)
O(2S)-H(2SB)···O12	0.8495(30)	1.9548(21)	2.7863(35)	165.8(1)
O(3S)-H(3SA)···O18	0.8507(28)	2.0102(19)	2.8175(33)	158.1(1)
O(3S)-H(3SB)···O14	0.8501(28)	1.9859(23)	2.8316(36)	173.0(1)
O(4S)-H(4SA)···O6	0.8509(30)	1.9710(19)	2.7902(35)	161.2(2)
O(4S)-H(4SB)···O10	0.8514(30)	2.0048(22)	2.8364(37)	165.2(2)
O(5S)-H(5SA)···O6	0.8494(24)	1.7503(19)	2.5757(30)	163.3(1)
O(5S)-H(5SB)···O10	0.8514(23)	1.9300(23)	2.7790(33)	174.8(1)
O(6S)-H(6SA)···O6	0.8492(28)	1.7807(19)	2.5732(32)	154.4(1)
O(6S)-H(6SB)···O3	0.8492(29)	1.9194(21)	2.7649(35)	173.5(1)
N(2)-H(2N) ···O(1S)	0.8608(32)	1.8238(32)	2.6733(46)	168.7(2)
N(3)-H(4N) ···O(4S)	0.8603(42)	1.8444(33)	2.7047(54)	179.5(2)
N(4)-H(4) ···O(3S)	0.8598(38)	1. 9493(30)	2.7090(49)	146.6(2)

Table II.5 O···O interactions in **1**.

O···O	**Bond distance (Å)**
O2···O23	2.7329(27)
O11···O24	2.7561(27)
O4···O21	2.6807(27)
O13···O20	2.6838(28)

II.3.1.2 Crystal Structure of 2

Solvent evaporation of Solution A (as shown in Scheme II.1) resulted in the crystallization of green block like crystals of $[\{Cr_3(O)(CH_3COO)_6(H_2O)_3\}_2\{H_7CrMo_6O_{24}\}].24H_2O$, **2**. The asymmetric unit of **2** consists of an Anderson-Evans cluster anion, $[H_7CrMo_6O_{24}]^{2-}$and the counter cation being a chromium trinuclear cluster, $[\{Cr_3(O)(CH_3COO)_6(H_2O)_3\}^{3+}$ as shown in Figure II.5. The inter cluster regions are occupied by twenty four lattice water molecules. Similar to the crystal structure of **1,** the Anderson cluster anion *viz.* $[H_7CrMo_6O_{24}]$, a B-type Anderson structure consist of six $[MoO_6]$ octahedra arranged in a hexagonal manner around the central $[Cr(OH)_6]$ octahedron (Figure II.5).The Mo-O distances in $[MoO_6]$ octahedra in **2** (Table II.6) ranges from 1.685(3)-1.709(2)Å for molybdenum-terminal oxygen (Mo-Ot), 1.935(3)-1.983(3) Å for molybdenum bridging oxygen (Mo-Ob) and 2.270(3)-2.314(3)Å for Mo-Oc bonds. The bond valence sum calculations suggested +3 oxidation state for Cr atoms and +6 oxidation state for all Mo atoms and protonation of seven oxygen atoms in **2**. Strong intermolecular hydrogen bonding interactions in **2** (2.462(4)-2.529(5) Å, Table II.7) between Anderson cluster and chromium acetate complex leads to 1-D chain (Figure II.6). The chains are further connected by inter chain H-bonding interactions (2.620(4)-2.641(4) Å) to form 2-D sheets as shown in Figure II.7. The packing of 2-D sheets into 3-D supramolecular structure is facilitated by lattice water molecules mediated by O···O

interactions (2.604(6)-3.090(6) Å) as shown in Figure II.8a. Figure II.8b shows the interaction of water molecules resulting in 1-D zig-zag chain in **2**.

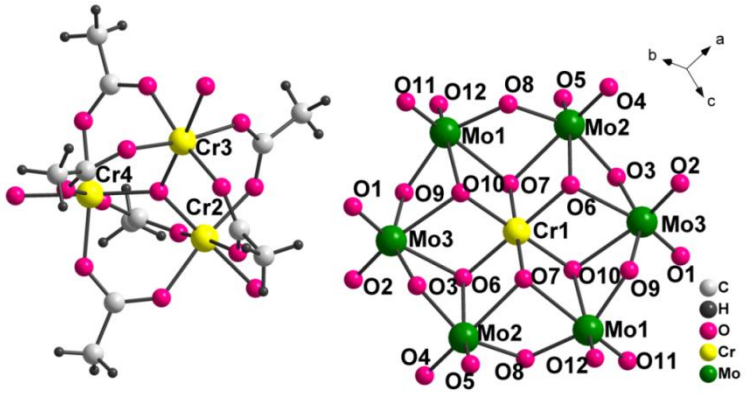

Figure II.5 Asymmetric unit in **2**. Lattice water molecules are omitted for clarity.

Table II.6 Mo-O distances in **2**.

Category	Mo···O	Bond Distance (Å)
Molybdenum-terminal oxygen (Mo-Ot)	Mo1···O11	1.689(3)
	Mo1···O12	1.704(3)
	Mo2···O4	1.697(3)
	Mo2···O5	1.707(3)
	Mo3···O1	1.685(3)
	Mo3···O2	1.709(2)
Molybdenum-bridging oxygen (Mo-Ob)	Mo1···O8	1.936(3)
	Mo1···O9	1.983(3)
	Mo2···O3	1.952(3)
	Mo2···O8	1.940(3)
	Mo3···O3	1.935(3)
	Mo3···O9	1.970(3)
Molybdenum-internal oxygen (Mo-Oc)	Mo1···O7	2.314(3)
	Mo1···O10	2.276(3)
	Mo2···O6	2.270(3)
	Mo2···O7	2.285(2)
	Mo3···O6	2.295(3)
	Mo3···O10	2.307(2)

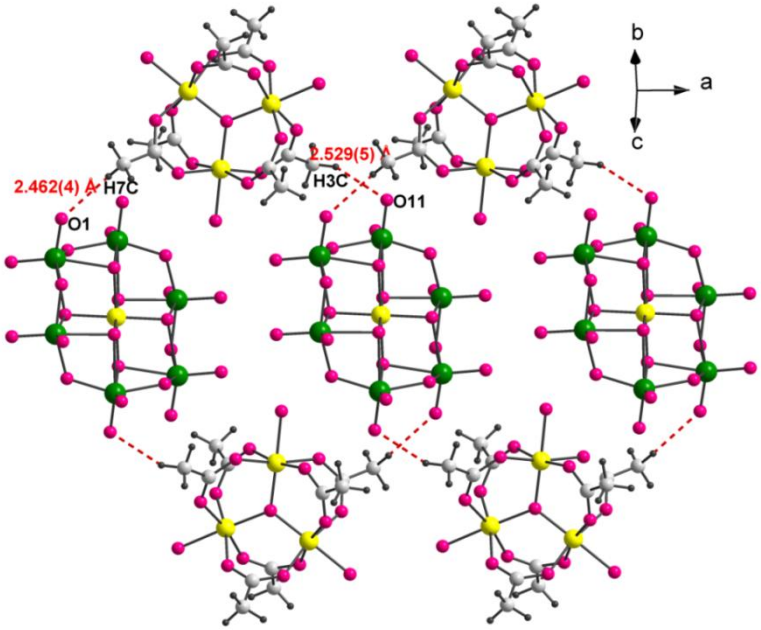

Figure II.6 Anderson clusters are connected by H-bonding interactions through chromium acetate complex to form 1-D chain.

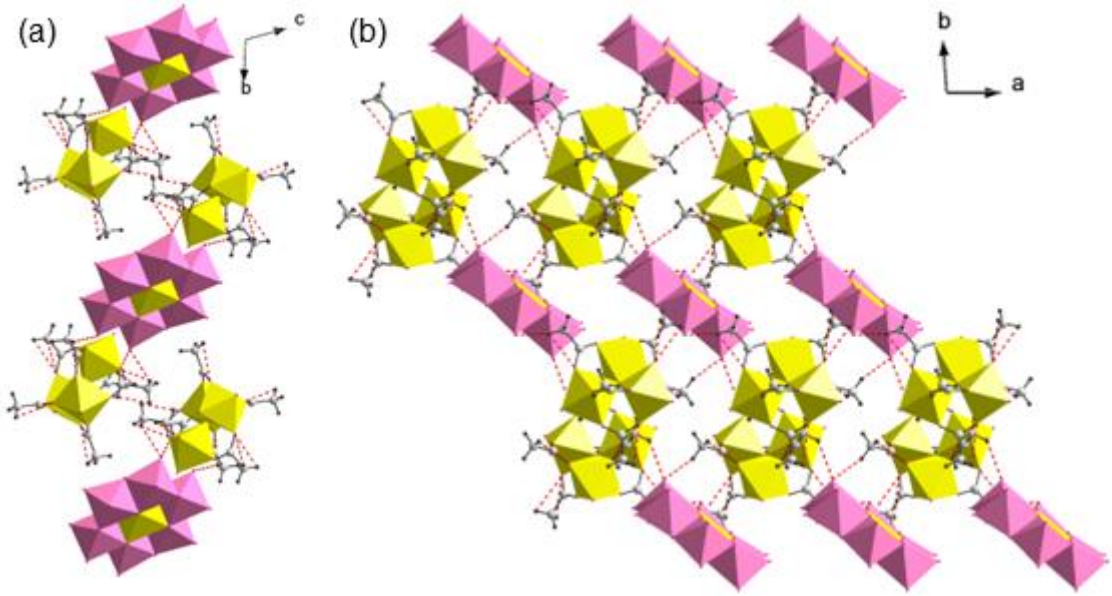

Figure II.7 (a) View along *a* axis showing 2-D sheets in **2** formed by H-bonding interactions between Anderson cluster and chromium acetate species. (b) View along *c* axis showing 2-D sheets in **2**.

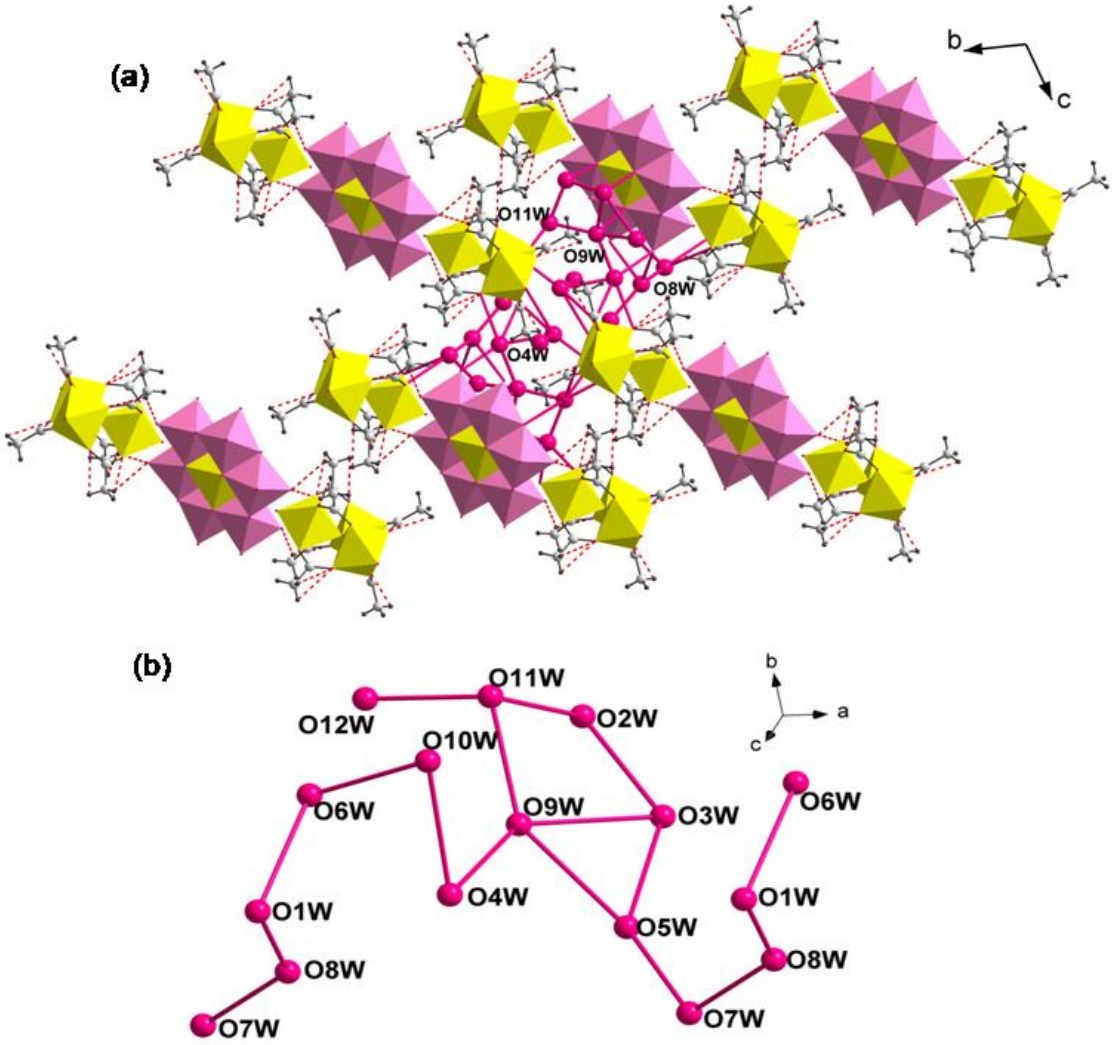

Figure II.8 (a) Two neighboring sheets are connected via hydrogen bonded clusters to form 3-D supramolecular structure. Lattice water molecules are shown in pink color and O···O interactions are shown in solid pink lines. (b) Water-water interactions resulting in 1-D zig-zag chain of water cluster in **2**.

Table II.7 H-bonding interactions in **2**.

D-H...A	**D-H (Å)**	**H...A (Å)**	**D...A (Å)**	**∠D-H...A (°)**
C3-H3C···O11	0.961(5)	2.529(5)	3.426(8)	155.44(3)
C7-H7C···O1	0.960(4)	2.462(4)	3.327(6)	149.81(2)
C9-H9B···O5	0.960(5)	2.641(4)	3.517(7)	151.99(3)
C1-H1A···O1	0.960(5)	2.620(4)	3.278(7)	126.13(2)
C3-H3A···O8	0.960(5)	2.777(6)	3.635(8)	149.37(2)
C1-H1A···O12W	0.960(5)	2.759(7)	3.539(9)	139.0(3)

Table II.8 O···O interactions in **2**.

O···O	Bond distance(Å)
O1w ···O8w	2.710
O7w···O8w	2.799
O6w···O8w	3.071
O6w···O10w	2.879
O4w···O10w	3.047
O4w···O9w	2.746
O5w···O9w	3.075
O5w···O7w	2.865
O9w···O11w	2.761
O3w···O5w	3.200
O3w···O9w	3.090
O2w···O3w	2.779
O2w···O11w	2.722
O11w···O12w	2.604

II.3.1.3 Crystal Structure of 3

The supernatant liquid after filtration of **2** was left undisturbed at room temperature and it resulted in the formation of pink crystals of $[Na\{Na(H_2O)_3\}_2\{H_6CrMo_6O_{24}\}].2H_2O$, **3**. It consists of Anderson cluster anion $[H_6CrMo_6O_{24}]^{3-}$ and hydrated sodium cations along with two lattice water molecules. Of the two sodium centers, Na2 is surrounded by lattice water molecules forming 1-D chains propagating along *c* axis (Figure II.9). Neighboring Na2 hydrate chains are connected by Anderson clusters to form 2-D sheets as shown in

Figure II.10. These neighboring 2-D sheets are further connected by sodium (Na1) hydrate complexes to form 3-D structure as shown in Figure II.11. The bond-valence calculations suggested that Cr atoms are in the +3 oxidation state and all Mo atoms are in the +6 oxidation state in **3**.

Table II.9 Mo-O distances in **3**.

Category	Mo···O	Bond Distance (Å)
Molybdenum-terminal oxygen (Mo-Ot)	Mo1···O1	1.694(2)
	Mo1···O2	1.708(3)
	Mo2···O3	1.709(3)
	Mo2···O4	1.718(2)
	Mo3···O5	1.696(2)
	Mo3···O6	1.685(2)
	Mo4···O7	1.695(1)
	Mo4···O8	1.707(3)
	Mo5···O9	1.703(3)
	Mo5···O10	1.709(2)
	Mo6···O11	1.699(2)
	Mo6···O12	1.696(2)
Molybdenum-bridging oxygen (Mo-Ob)	Mo1···O13	1.907(1)
	Mo1···O14	1.951(2)
	Mo2···O14	1.956(1)
	Mo2···O15	1.904(3)
	Mo3···O15	1.945(3)
	Mo3···O16	1.934(4)
	Mo4···O16	1.919(1)
	Mo4···O17	1.940(2)
	Mo5···O17	1.946(1)
	Mo5···O18	1.918(3)
	Mo6···O13	1.959(4)
	Mo6···O18	1.931(3)
Molybdenum-internal oxygen (Mo-Oc)	Mo1···O20	2.293(4)
	Mo1···O10	2.276(3)
	Mo1···O21	2.260(3)
	Mo2···O21	2.263(1)
	Mo2···O22	2.302(5)
	Mo3···O22	2.372(2)
	Mo3···O23	2.300(1)
	Mo4···O23	2.289(4)
	Mo4···O24	2.306(3)
	Mo5···O24	2.287(1)
	Mo5···O19	2.301(5)
	Mo6···O19	2.295(2)
	Mo6···O20	2.293(1)

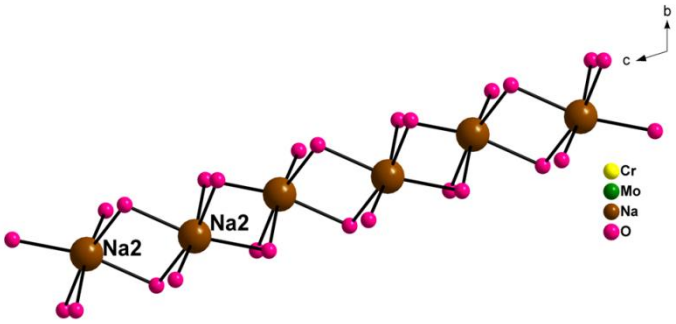

Figure II.9 Two sodium centers (Na2) connected by lattice water molecules forming 1-D chains propagating along *c* axis in **3**.

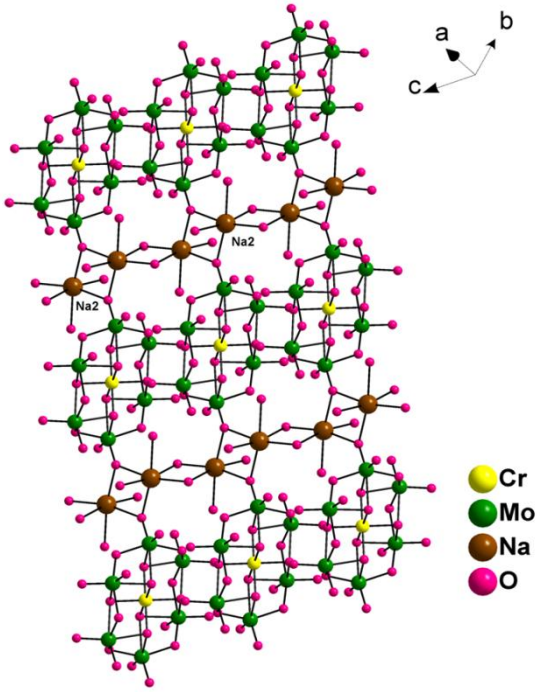

Figure II.10 Neighboring Na2 hydrate chains are connected by Anderson clusters to form 2-D sheets in **3**.

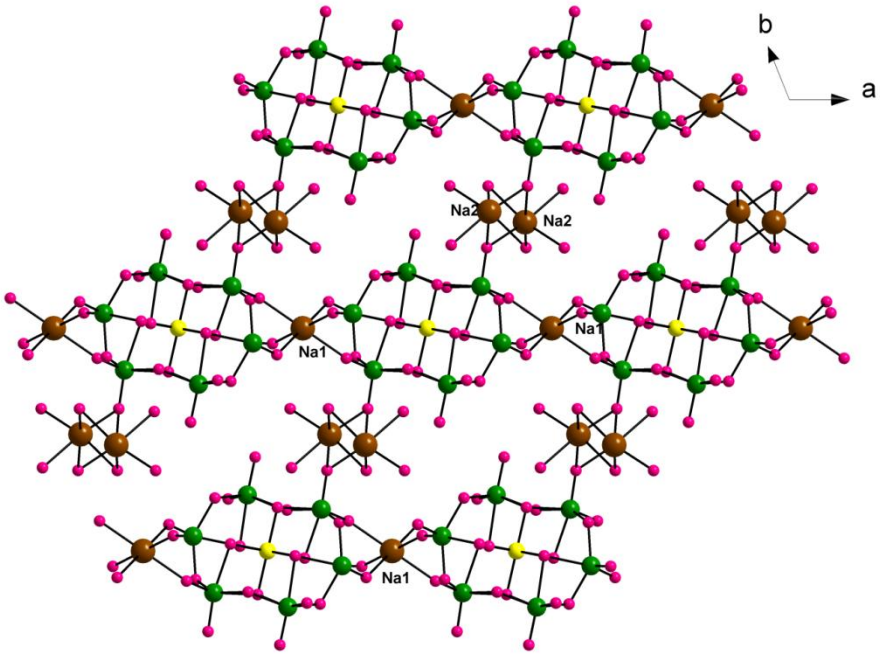

Figure II.11 2-D sheets are connected by sodium (Na1) hydrate complexes to form 3-D structure.

II.3.2 Vibrational and Thermal Analysis

The FTIR spectra of solids **1-3** displayed similar vibrations which are characteristic of the Anderson-type structure (Figure II.12). Vibrational bands were observed between 890 and 950 cm^{-1} for the Mo-Ot bonds, between 660 and 740 cm^{-1} for the Mo-Ob groups, and between 400 and 600 cm^{-1} for the Mo-Oc groups. In **1**, peaks in the range 3000-3300 cm^{-1} could be attributed to stretching vibrations of the N-H group in the pyrazole moiety. Peaks at 1621 and 1517 cm^{-1} corresponded to C-N stretching and N-H bending vibrations respectively. In **2**, strong bands at 1612 and 1456 cm^{-1}were attributed to $\nu_{as}(CO_2)$ and ν_s (CO_2) modes, respectively of the bridging acetic acid groups and strong band observed at 665 cm^{-1} were attributed to the $\nu_{as}(Cr_3O)$ vibration. **3** also showed IR spectra characteristics of the Anderson cluster anion.

TG analysis of **1** (FigureII.13a) showed weight loss in three steps. In **1**, the first weight loss upto 110°C corresponding to 8.9% was due to loss of six lattice water molecules

(calcd. 8.6%). The thermal degradation of two pyrazole moieties could be accounted for the second weight loss of 11.4% upto350°C (calcd. 10.9%). Subsequent loss could be assigned to the decomposition of $\{CrMo_6O_{24}\}$ cluster anion.TGA of solids **2** and **3** showed the weight loss in multiple steps wherein the first step was due to loss of lattice water molecules. In **2**, weight loss in next step was observed corresponding to the loss of chromium trinuclear complex, followed by degradation of Anderson cluster (Figure II.13b). **3** showed loss of lattice water molecules and degradation of Anderson cluster (Figure II.13c).

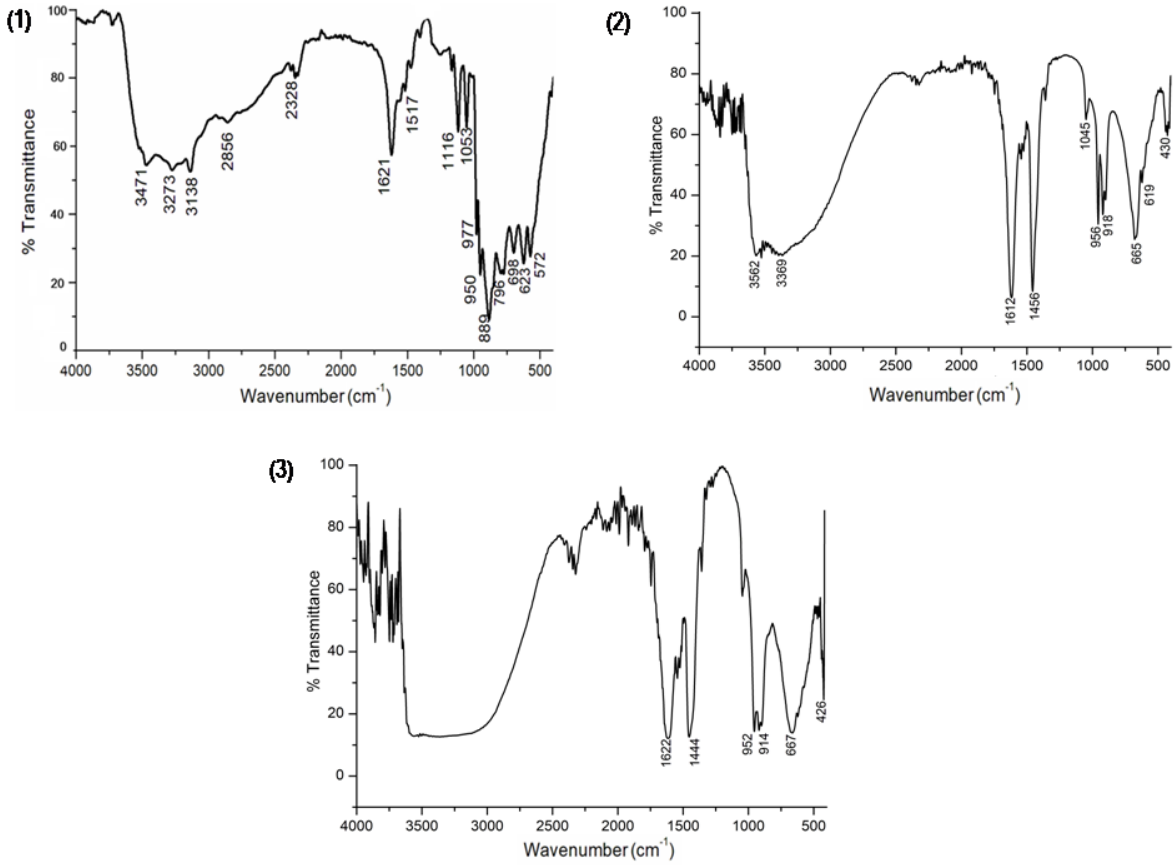

Figure II.12 FTIR spectra of solids **1, 2** and **3**.

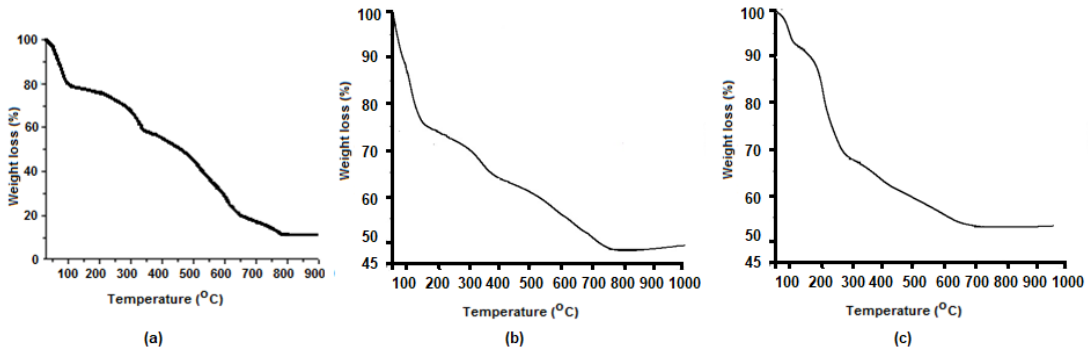

Figure II.13 TG analysis plot of (a) **1**, (b) **2** and (c) **3.**

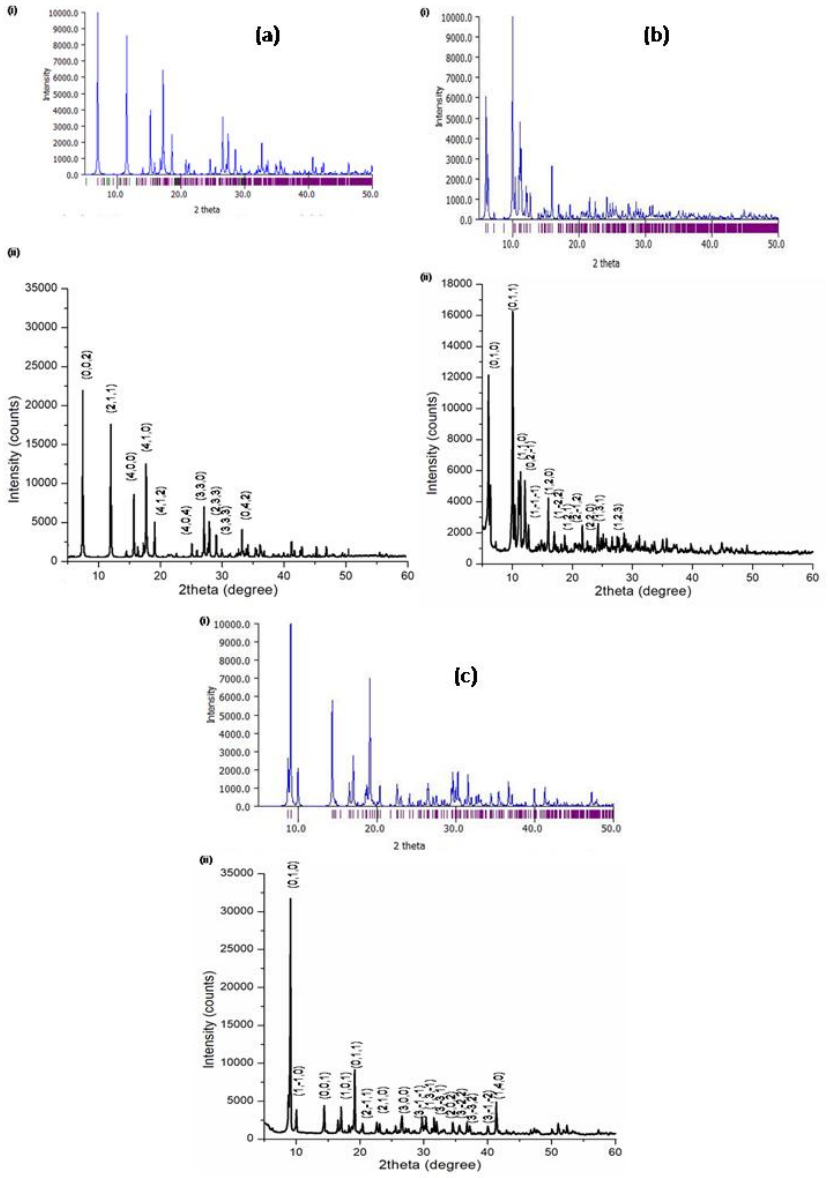

Figure II.14 (i) Simulated and (ii) experimental powder X-ray patterns of (a) **1**, (b) **2** and (c) **3.**

II.3.3 Chemistry of Formation

Self-assembly of Anderson-Evans cluster based solids usually occurs via solvent evaporation technique under acidic conditions. The synthetic methodology used in the current investigation involved mixing of aqueous molybdate solution containing chromium ions with a solution of cobalt ions in the presence of an organic ligand *viz*. pyrazole, under constant stirring. Once the two solutions were mixed, the solution was further acidified using HCl. Finally, the resultant solution when left undisturbed resulted in crystallization of solid **1**. The addition of HCl resulted in a decrease in the pH of the reaction medium and provided large number of protons in the solution. Therefore, the addition of HCl had a twofold effect. Firstly, the highly acidic pH favored the formation of protonated $[Hx(XO_6)M_6O_{18}]^{(9-x)-}$ cluster species and secondly, it resulted in the protonation of the organic ligands. Therefore, in the case of **1**, the increase in positively charged organic moieties $(H\textit{pz})^+$ (pKa of pyrazole: 2.1[29]) inhibited cobalt-pyrazole interaction resulting in an organically templated hybrid solid $[\{H\textit{pz}\}_2\{H_7CrMo_6O_{24}\}]\cdot 6H_2O$ (**1**). Additionally, the crystal structure of **1** also showed the presence of six lattice water molecules. Earlier it has been demonstrated in several examples that aggregation of water cluster is a secondary factor in the crystal packing of such complex structures [16]. Protonation of Anderson-Evans cluster anion and synthesis under ambient conditions are the key factors that seem to be responsible for the aggregation of water molecules in cluster based solids. A close examination of results reported in literature (Table II.1) also suggested that Anderson-Evans cluster based solids synthesized under hydrothermal conditions were less hydrated as compared to those obtained via solvent evaporation technique.

When solution **A** consisting of sodium molybdate, chromium chloride and acetic acid was allowed to evaporate at room temperature, it resulted in the formation of **2** and **3.** The

presence of acetic acid favored the formation of chromium acetate trinuclear complex which acted as a counter cation to the Anderson cluster anion, **2**. Since most of the chromium ions were utilized during the crystallization of **2**, the remaining Anderson anions aggregate along with sodium ions to form hydrated Anderson cluster, **3**.

II.3.4 Synthesis of Polypyrrole and Polypyrrole composite using Solids 1-3

Polypyrrole, a conductive polymer, has gained immense attention owing to its interesting properties and wide range of applications [30]. One of the simple and feasible methods for the synthesis of Polypyrrole (Ppy) is by chemical oxidative polymerization of pyrrole monomer. Various oxidizing agents like ferric chloride ($FeCl_3$), ammonium persulphate (APS), etc. are commonly used for polymerization [31]. Polyoxometalates, especially those containing molybdenum, have also been used in the synthesis of polymers or polymer composites since they can provide sufficient oxidizing medium for oxidative polymerization and can even form composite materials with the polymer [32]. Based on these considerations, Anderson cluster based solids **2** and **3** were examined for the formation of Polypyrrole and Polypyrrole composite through oxidative polymerization of pyrrole. Use of solid **1** was avoided as it already had an organic component incorporated in it which could hinder the polymerization process.

Ppy was successfully synthesized using APS in presence of Anderson cluster solid $[\{Cr_3(O)(CH_3COO)_6(H_2O)_3\}_2\{H_7CrMo_6O_{24}\}].24H_2O$, **2** as per the procedure described in Section II.2.2. FTIR spectrum showed bands characteristics of the pyrrole ring (refer Figure II.15a). The formation of polypyrrole was further confirmed from the PXRD patterns of the synthesized polymer. X-ray diffraction pattern of synthesized polypyrrole showed a broad peak at $2\theta=26°$, which is characteristic peak of amorphous polypyrrole [33] as observed in Figure II.15b. Polymerization of pyrrole was also carried out using

Solid **2** without APS and also using only APS as the oxidizing agent. In the later case polypyrrole was obtained, but the yield was very less when synthesis was carried out using only APS (i.e. in the absence of **2**). When solid **3** was used for polymerization of pyrrole, it resulted in the formation of Ppy along with traces of Anderson solid **3** which was confirmed from the PXRD pattern as shown in Figure II.16 indicating the formation of a composite material.

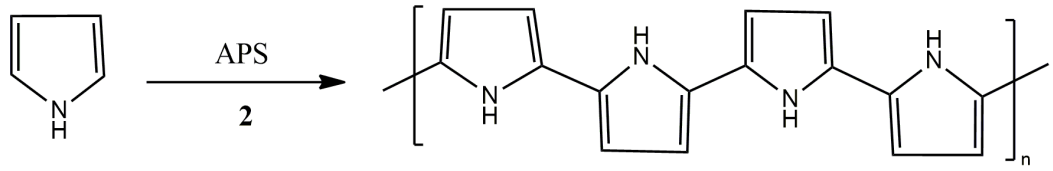

APS = $(NH_4)_2S_2O_8$

2 = $[\{Cr_3(O)(CH_3COO)_6(H_2O)_3\}_2\{H_7CrMo_6O_{24}\}]\cdot 24H_2O$

Scheme II.2 Formation of Polypyrrole using APS and solid **2.**

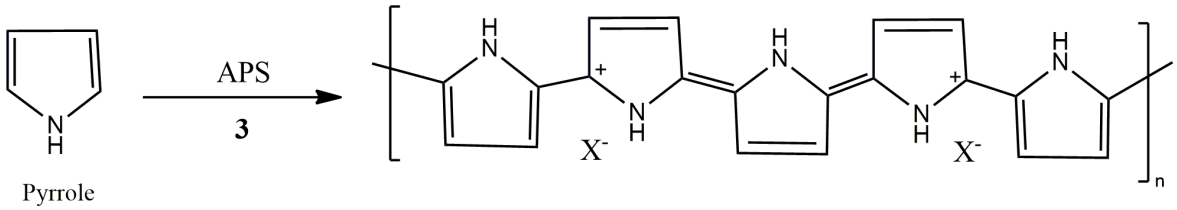

APS = $(NH_4)_2S_2O_8$

3 = $[Na\{Na(H_2O)_3\}_2\{H_6CrMo_6O_{24}\}]\cdot 2H_2O$

X = $\{H_6CrMo_6O_{24}\}$

Scheme II.3 Formation of Anderson-Polypyrrole composite using APS and solid **3.**

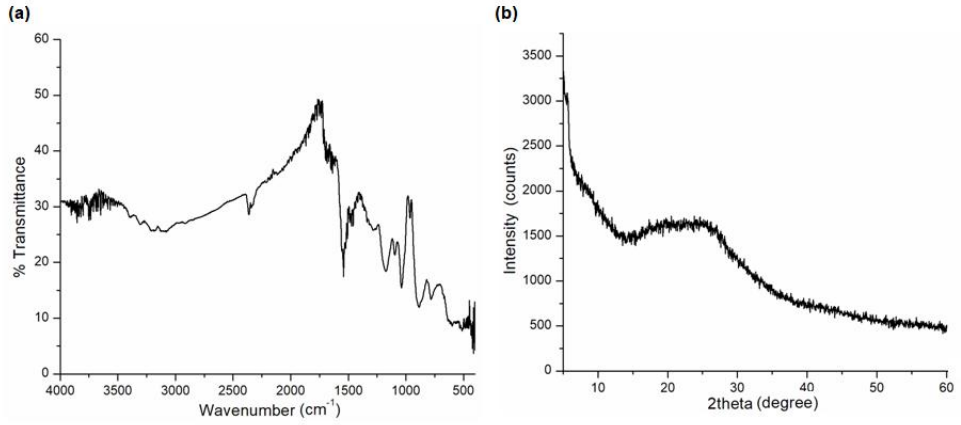

Figure II.15 (a) FTIR spectrum and (b) PXRD pattern of Polypyrrole synthesized using APS and Solid **2**.

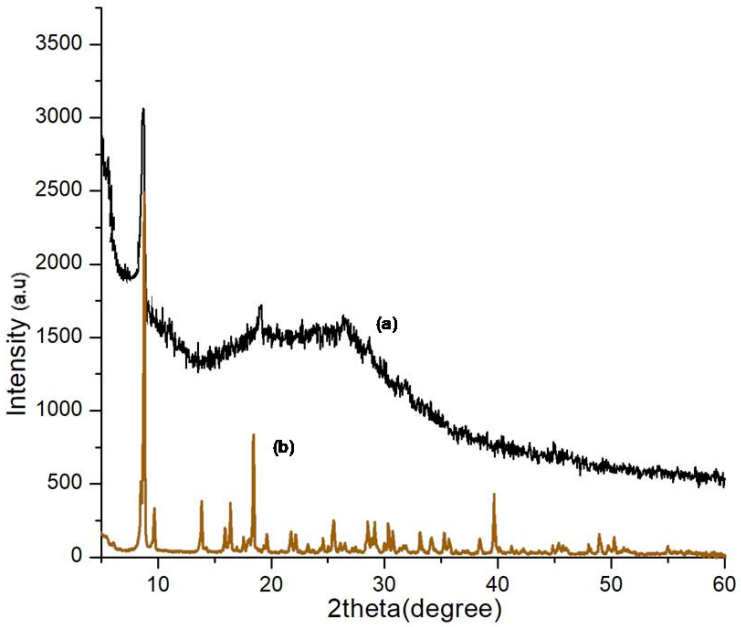

Figure II.16 (a) PXRD pattern of product synthesized using APS and solid **3**, (b) PXRD pattern of Anderson cluster, **3.**

II.4 Conclusions

Anderson-Evans type polyoxomolybdate solids **1-3** have been crystallized via solvent evaporation technique. Solvent evaporation technique offers a facile method for the synthesis of hybrid solids. Subtle changes in reaction parameters can affect the nature of

molecular precursors in solution and offer alternative pathway for the crystallization of new phases. Detailed structural analysis revealed the role of supramolecular interactions in the crystal packing of solids. The hydrogen bonding interactions mediated by organic cations in **1** and by lattice water molecules in all the three solids plays a significant role in stabilizing the crystal packing. The ability of solids **2** and **3** for the synthesis of Polypyrrole and Polypyrrole composite using oxidative polymerization method was investigated. Anderson cluster based solids were found to be promising candidates for effective polymerization of pyrrole and for preparing polymer based composite materials.

References

1. Ariga K, Hill JP, Lee MV, Vinu A, Charvet R, Acharya S (2008) Sci Technol Adv Mater 9:014109
2. Lazzari M, Rodríguez-Abreu C, Rivas J, López-Quintela M (2006) J Nanosci Nanotechnol 6(4):892-905
3. Elemans JAAW, Rowan AE, Nolte RJM (2003) J Mater Chem 13:2661-2670
4. Misra A, Kozma K, Streb C, Nyman M (2020) Angew Chem Int Ed 59:596-612
5. Pradeep CP, Long DL, Cronin L (2010) Dalton Trans 39:9443-9457
6. Wang X, Vittal JJ (2003) Inorg Chem 42:5135-5142
7. Blazevic A, Rompel A (2016) Coord Chem Rev 307:42-64
8. Cindrić M, Veksli Z, Kamenar B (2009) Croat Chem Acta 82:345-362
9. Wu P, Wang Y, Huang B, Xiao Z (2021) Nanoscale 13:7119-7133
10. Ali Khan M, Shakoor Z, Akhtar T, Sajid M, Asif HM (2021) Inorg Chem Commun 133:108875
11. An H, Li Y, Xiao D, Wang E, Sun C (2006) Cryst Growth Des 6:1107-1112
12. Jin P, Wei H, Zhou L, Wei D, Wen Y, Zhao B, Wang X, Li B (2021) Mol Catal 510:111705
13. Boulmier A, Vacher A, Zang D, Yang S, Saad A, Marrot J, Oms O, Mialane P, Ledoux I, Ruhlmann L, Lorcy D, Dolbecq A (2018) Inorg Chem 57:3742-3752
14. Kumar D, Ahmad S, Prakash GV, Ramanujachary KV, Ramanan A (2014) Cryst Eng Comm 16:7097-7105
15. Yang YY, Song Y, Liu LY, Qu XS (2011) Acta Cryst E67:m776
16. Singh M, Kumar D, Ramanan A (2014) Proc Natl Acad Sci India Sect A Phys Sci 84:305-314
17. Ouahab L, Golhen S, Yoshida Y, Saito G (2003) J Clust Sci 14:193-204

18. Wang SM, Li YW, Feng XJ, Li YG, Wang EB (2010) Inorg Chim Acta 363:1556-1560

19. Wu XJ, Shen XM, Zhang P, Deng Q, Lü SZ, Cai TJ (2011) Z. Kristallogr New Cryst Struct 226:387

20. Peng ZS, Zhang CL, Shen XM, Deng Q, Cat TJ (2011) J Coord Chem 64:2848-2858

21. Yang YY, Song Y, Liu LY, Qu XS (2011) Acta Crystallogr Sect E Struct Rep Online 67(Pt 6):m776

22. Li XM, Guo Y, Shi T, Chen YG (2016) J Clust Sci 27:1913-1922

23. Pavani K: Transition metal complex templated polyoxomolybdates: synthesis, structure and magnetism. Indian Institute of Technology, Delhi, India (2007)

24. Bruker Analytical X-ray Systems (2000) SMART: Bruker Molecular Analysis Research Tool, Version 5.618

25. Bruker Analytical X-ray Systems (2000) SAINT-NT, Version 6.04

26. Bruker Analytical X-ray Systems (2014) SHELXTL

27. Klaus B, University of Bonn, Germany DIAMOND, Version 4.1

28. Brown ID, Altermatt D (1985) Acta Crystallogr B 41:244-247

29. Dewick PM (2006) Essentials of Organic Chemistry: For Students of Pharmacy, Medicinal Chemistry and Biological Chemistry, John Wiley & Sons Ltd, England

30. Hao L, Dong C, Zhang L, Zhu K, Yu D (2022) Polymers 14:5139

31. Zhang X, Zhang J, Song W, Liu Z (2006) J Phys Chem B 110:1158-1165

32. Gómez-Romero P, Casañ-Pastor N, Lira-Cantú M (1997) Solid State Ionics 101-103: 875-880

33. Chaluvaraju BV, Sangappa KG, Murugendrappa MV (2015) Polym Sci Ser A 57:467-472